Adopting the topology optimization in the design of high-speed synchronous reluctance motors for electric vehicles

Andrea Credo
Student Member, IEEE
University of L'Aquila
L'Aquila, Italy
andrea.credo@graduate.univaq.it

Giuseppe Fabri
Member, IEEE
University of L'Aquila
L'Aquila, Italy
giuseppe.fabri@univaq.it

Marco Villani
University of L'Aquila
L'Aquila, Italy
marco.villani@univaq.it

Mircea Popescu
Fellow, IEEE
Motor Design Limited
Wrexham, UK
mircea.popescu@motor-design.com

***Abstract* -- This paper deals with the design of high-speed Synchronous Reluctance motors for electric vehicle applications. The need to enhance the power density and to lower the cost leads to research on high-speed motors with a reduced amount of rare earth. Pure Synchronous Reluctance motors potentially operate at high speed and exhibit a cost-effective rotor compared to PM and induction motors. Nevertheless, they present reduced performances in deep flux weakening operations, in particular when the so-called radial ribs are introduced to increase the mechanical robustness of the rotor. In this paper the introduction of the radial ribs and the related design challenges are investigated and discussed. The adoption of the topology optimization tool that is able to optimize the amount, the positioning and the sizing of suitable structural ribs is presented. A design flow integrating the Topology Optimization is presented. The approach leads to an original positioning of the radial ribs able to preserve the performance of the motor at high operating speed enhancing the mechanical integrity of the rotor.**

***Index Terms* -- synchronous reluctance machine, e-mobility, high-speed, rare earth free, mechanical analysis, optimized ribs, topology optimization, multiphysics approach.**

I. INTRODUCTION

The electric machines have become the primary candidate for mobility [1]-[3], adopting motor solutions mainly based on high performance permanent magnets (PM) manufactured with Rare-Earth (RE) materials [4]-[6].

The imminent mass production of Electric Vehicles (EV) arises concerns related to RE price volatility, their supply risks and their sustainable extraction. Therefore, there is a growing attention on alternative solutions that include RE free machines or reduced RE machines [7]. In this context, the designers are pushed to increase the maximum operating speed of motor-drives to enhance the specific power, above all in absence of powerful RE magnets [8].

The previous considerations are supported by Table I, in which the motors with a higher maximum speed are the RE free motors, such as the Induction Motor and the PMA SynRel. The Table I summarizes the main EVs sold in the EU & US markets, reporting the adopted technological solution for traction motors, the maximum operating speed and the main powertrain data, which are based on [6] and [9]. The maximum speed has been estimated by the authors when not available.

Synchronous Reluctance Motors (SynRels) are becoming of great interest in the recent years, due to their potential cost effectiveness, efficiency and performance [10], [11], [12].

When compared to PM motors, conventional SynRels are known for their lower specific (peak) power and specific (peak) torque, higher noise and lower power factor. Nevertheless, adequate performances can be achieved through an optimized rotor design [13], [14], [15].

In particular, to compete with PM motors, the specific power in SynRels is enhanced by increasing the rotor operating speed and the flux-weakening region. The optimal electromagnetic rotor geometry for performance enhancement is challenging to adopt due to mechanical integrity issues at high speed. The so-called "ribs" (Fig. 1) are usually included in tangential and radial directions in SynRel's rotor geometry. They reduce the mechanical stress in the rotor core and limit the maximum deformation at the airgap due to centrifugal forces. However, the motor performance is negatively affected by these ribs [16].

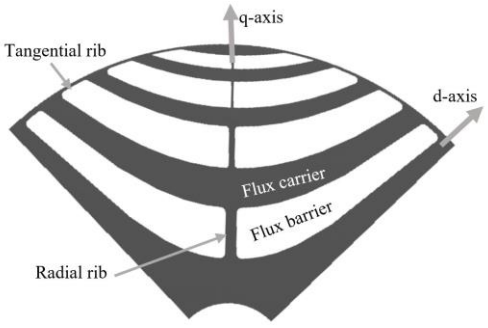

Fig. 1. Typical geometry of the SynRel rotor with flux barriers and ribs.

The paper proposes the adoption of a Topology Optimization (TO) in the challenging trade-off between the electromagnetic and mechanical design aspects of SynRels.

The paper is organized as follows: section II describes the requirements of the motor with reference to a high-speed liquid-cooled SynRel for full-electric premium vehicles and proposes a suitable electromagnetic design. Section III discusses the possible approaches to guarantee the rotor mechanical integrity at high speed focusing on the adoption of structural ribs. Section IV proposes the optimization of the structural ribs by using a TO and the obtained results are discussed in Section V. Final remarks are drawn in the Conclusions.

TABLE I
TRACTION MOTORS FOR ELECTRIC VEHICLES (2018-2019)

Vehicle Model	Motor type Front / Rear	Max Power (kW) Front / Rear	Top speed (km/h)	Acceleration 0-100 km/h (s)	Transmission ratio	EM Max speed (rpm)	Battery energy (kWh)
Audi e-tron 55	IM / IM	125 / 140	200	6.6	9.2	13000	95
Audi Q4 e-tron	IM / PMSM	75 / 150	180	6.3	9.2	12000	82
BMW i3S 42	- / PMASynRel	- / 135	160	6.9	9.66	11500	42.2
BMW i3S 33	- / PMASynRel	- / 135	160	6.9	9.66	11500	33.2
Chevrolet Bolt	PMSM / -	150 /-	145	6.9	7.05	8600	60
FIAT 500e	PMSM / -	83 /-	141	-	9.59	12000	24
Hyundai e-Kona 64	PMSM / -	150 /-	167	7.6	7.98	10500	64
Jaguar I-Pace	PMSM / PMSM	147 / 147	200	4.8	9.04	13000	90
KIA Soul EV	PMSM / -	81 / -	145	11.5	8.21	9600	31.8
KIA e-Niro 39	PMSM / -	100/ -	155	9.8	8.21	10000	39.2
KIA e-Niro 64	PMSM / -	150 / -	167	7.8	8.21	11000	64
Nissan Leaf SL Plus	PMSM / -	160 / -	159	-	8.19	10500	62
Nissan Leaf SL	PMSM / -	110 / -	144	7.9	8.19	9700	40
Renault Zoe R110	WRSM / -	80 / -	135	11.4	9.3	11000	45.6
Renault Zoe Q90	WRSM / -	65 / -	135	13.2	9.3	11000	45.6
Tesla Model X	IM / IM	193 / 375	250	3.7	9.7	17000	100
Tesla Model X SR	PMASynRel / IM	193 / 375	250	2.9	9.7	17000	100
Tesla Model 3	IM / PMASynRel	147 / 211	261	3.4	9.7	20000	79.5
Tesla Model S P100D	IM / IM	193 / 375	250	2.4	9.7	18000	100
Volkswagen e-Golf	PMSM / -	100 / -	150	9.6	9.7	12000	35.8
Volkswagen e-up!	PMSM / -	60 / -	130	12.4	8.16	10000	18.7

PMSM = PM Synchronous Motor; IM = Induction Motor; PMASynRel = Permanent Magnet Assisted Synchronous Reluctance Motor; WRSM = Wound Rotor Synchronous Motor

II. Optimized Electromagnetic Design of Synchronous Reluctance Motors

The design of the SynRel for traction applications requires accurate sizing procedures that differ from the process of an industrial machine, which is designed to mostly operate at rated speed and torque. In traction motors, specific tools and optimization procedures [17]-[19] become essential tools for the design refinement in order to satisfy the challenging requirements over a wide speed range.

Table II reports the application requirements related to a premium EV. It is worth noting that at the base speed (5000 rpm) a high value of torque is requested; moreover, when the motor operates at the maximum speed (18000 rpm) a significant amount of power is needed. The SynRel works in a deep flux weakening condition (the max-speed base-speed ratio is 3.6). Moreover, the high value of the maximum required speed of the motor is relevant for the specified diameters and it is above the state of art in Table I.

A high-voltage battery (800V) has been selected to exploit the characteristics of the latest 1200V power modules and sustain the performance of the machine at high speed [20].

To reach the severe requirements in Table II it is useful to remind that the design of SynRels relies on the maximization of the saliency ratio (L_d/L_q), achieved by shaping the rotor geometry with several flux barriers per pole [21]. Tangential ribs are usually included in the optimal electromagnetic design for manufacturing reasons (Fig.1).

The saliency ratio and the electromechanical torque also depend on the number of poles and different combinations of slots/poles need to be evaluated.

In order to reduce the q-axis inductance maintaining the same d-axis inductance and according to [22], a low number of poles can be chosen; however, this choice increases the torque ripple. Therefore, the 2-pole machine maximizes the saliency ratio with a higher torque ripple.

Although this is true, the machines with a lower number of poles have a larger stator yoke that reduces the torque density; otherwise for a high number of poles it is hard to arrange a high number of flux barriers, penalizing the saliency ratio. It follows that the number of poles adopted in this type of applications is usually between 4 and 8.

In [1] different numbers of poles have been analyzed, optimized and compared (respectively 4, 6, and 8), concluding that the 6-pole design presents the best performance.

About the barrier shape, “fluid shape” or “Joukowsky barriers” have been chosen [23]. This type of shape offers benefits in routing the d-axis flux increasing the direct inductance, while it has the same behavior of other types of barriers (circular and rectangular) in the obstruction of the q-axis flux. Globally, the adoption of fluid shape presents a reduced torque ripple and advantages in the optimization steps.

TABLE II
Motor Requirements for the Target Application

Requirements		Constraints
DC Voltage	V	800
Specific Peak Power	kW/kg	> 4.0
Specific Peak Torque	Nm/kg	> 8.0
Peak Power	kW	200
Peak Torque	Nm	380
Peak Efficiency	%	> 95
Maximum Speed	rpm	18000
Power @ Max Speed	kW	>50
Motor Mass	kg	< 50
Outer Stator Diameter	mm	<250
Stack Length	mm	<220

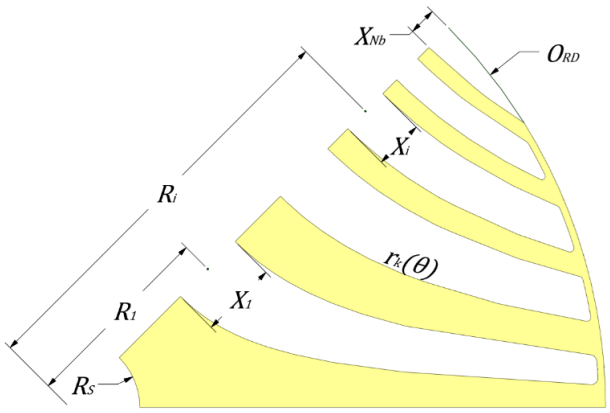

Fig. 2. Fluid-shaped rotor barriers (half pole) and design variables.

The variables that are useful for the definition of the rotor shape are shown in the Fig. 2 above.

The analytical expression of these barriers is computed from the Joukowsky (or Zhukovsky) equation:

$$r_k(\theta) = R_s \sqrt[p]{\frac{c_k + \sqrt{c_k^2 + 4\sin^2(p\theta)}}{2\sin(p\theta)}} \quad (1)$$

$$c_k = \frac{\left(\frac{R_i + (-1)^k X_i}{R_s}\right)^{2p} - 1}{\left(\frac{R_i (-1)^k X_i}{R_s}\right)^{p}} \quad (2)$$

$$\{k = 1, \dots, 2N_b - 1\} \qquad i = ceil\left(\frac{k}{2}\right)$$

where:
R_s is the radius of the shaft
c_k is a constant, function of the position and the thickness of the barriers
p is the number of pole pairs
θ is the mechanical angle
R_i is the position of the *i-th* barrier
X_i is the width of the *i-th* barrier
$r(\theta)$ is the radius of the barrier curve
N_b is the number of the barriers including the notch
$ceil$ is the function that gives the least integer greater than or equal to the input.

To design each barrier, it is necessary to define two curves and each curve is defined by a proper constant *c*. Since the usage of the Joukowsky equation is, as a matter of fact, a pre-optimization of the shape of the barriers, a preliminary design can be easily carried out.

The approach is effective even in the next optimization steps of the rotor geometry; using the fluid shape rotor, the number of variables is contained, the results are very promising, and the computational effort is acceptable.

The pure electromagnetic optimization uses a total of 16 variables, where the constraints are the peak power and the motor mass: the objective functions are the power at maximum speed and the motor efficiency.

In detail, nine variables are related to the rotor: two for each barrier (X_i, R_i) and one for the notch (X_{N_b}). Four variables for the stator: tooth width, yoke height, number of slots per phase per pole and number of conductors per slot. Three variables are general: stack length, current amplitude, and current angle.

The design data of the optimized solution are listed in Table III. It reports the main dimensions of the stator and the rotor, and the main performance required by the automotive application (Table II).

The cross section of the 6-pole design, optimized from the electromagnetic point of view, is shown in Fig. 3. The tangential ribs, supporting the flux carriers, have a low impact on the performance. They are reported in this design only for completeness, but they are not used in the electromagnetic optimization.


Fig. 3. Cross section of the magnetically optimized design.

TABLE III
DESIGN DATA AND MAIN PERFORMANCE

Performance		**Value**
Outer Stator diameter	mm	220
Stack length	mm	200
Inner stator diameter	mm	152
Ribs thickness	mm	0.5
Number of conductors per slot	-	7
Slot fill factor	-	0.4
Airgap length	mm	0.7
Peak Power	kW	322
Power density	kW/kg	6.85
Peak Torque	Nm	430
Torque density	Nm/kg	9.15
Peak efficiency	%	97.4
Power @ max speed (18000 rpm)	kW	150
Max phase current	A	700
Current density @ rated power	A/mm^2	11.0
Maximum phase voltage	V	400
Motor mass	kg	47
Electrical steel		M235-35A
Lamination thickness	mm	0.35
Yield strength	MPa	455
Tensile strength	MPa	550

III. Rotor Design Criteria for High-Speed SynRels

After the electromagnetic optimization, the rotor geometry needs to be refined from the mechanical point of view because it is necessary to guarantee the integrity of the rotor over the full operating conditions. The focus needs to be on the mechanical stress and on the deformation at the airgap caused by the centrifugal forces.

The structure in Fig. 3 is retained only by the thin tangential ribs. The mass and the position of the rotor steel generate high centrifugal forces at high speed, causing great stress on the tangential ribs. The equivalent von Mises stress in the ribs already reach the ultimate tensile strength of the adopted electrical steel (550MPa) at 4500 rpm.

Different approaches are adopted in literature to mechanically improve the rotor retention with respect to centrifugal forces. The main ones are:

- Adoption of high strength electrical steel [24]: usually involves steels with lower magnetic properties;
- Adoption of retaining sleeves [25]: it is problematic since it would require a material substantially stiffer than steel to decrease the radial deflection under inertial load;
- Novel rotor constructions [26]: they need custom manufacturing process and custom spare parts;
- Adopting properly rotor interconnecting end plates or interconnecting shaft (dovetails vs press fit) [27]: it is more effective for compact buried PM rotors;
- Adoption of structural non-magnetic materials (epoxy resins, titanium, others) [25],[28],[29]; these are difficult to be interconnected with the rotor laminations and have an additional cost that has to be accurately evaluated;
- Adoption of optimized structural ribs [1],[16],[30],[31]: this is one of the most studied research topics in SynRel and PM machines because the adoption of the ribs deteriorates the electromagnetic performance.

Considering the adoption of structural ribs, the approach is to increase the thickness of the tangential ribs and to include radial ribs in the rotor barriers, starting from the inner ones, to retain the rotor's flux carriers. The number and the thickness of the ribs per pole increase significantly with the rotor speed.

After the optimal electromagnetic shape has been frozen, a mechanical optimization of the thickness of the ribs under centrifugal forces has been carried out. The structural optimization has been done by imposing as boundary conditions the allowable stress (under the yield strength) for the adopted electrical steel and the maximum deformation at the airgap. In detail, the total thickness of the ribs per flux barrier (tangential and radial) has been used as an objective function. This structural optimization allows to minimize the impact of the radial ribs on the machine performance. The optimized rotor geometry is shown in Fig. 4 with the computed equivalent von-Mises stress.

The performance of the motor is degraded by the insertion of the ribs, as expected; the details are provided in Section V, in which it can be seen the comparison between the optimal electromagnetic design and the ones with radial ribs and optimized ribs respectively.

While the barrier shape has not been modified compared to the optimal shape for the flux, the introduction of the ribs affects the magnetic behavior of the rotor and it globally reduces the motor performance. This happens because a large part of the magnetic flux flows through these ribs, increasing the quadrature inductance (L_q).

This effect is more significant in traction applications, where the electric motor usually operates in heavy flux-weakening conditions, in which the quadrature current is predominant with respect to the direct one, restricting the voltage limit. Moreover, in premium vehicles the motor power required at low speeds and the one required at maximum speed are conflicting requirements.

Additionally, the presence of radial and tangential ribs increases the magnetic coupling between direct and quadrature axes, affecting the effectiveness of the control strategy. This leads to a reduction of the motor performances unless a non-linear model obtained by Finite Elements (FE) computation is used in the control algorithm [32].

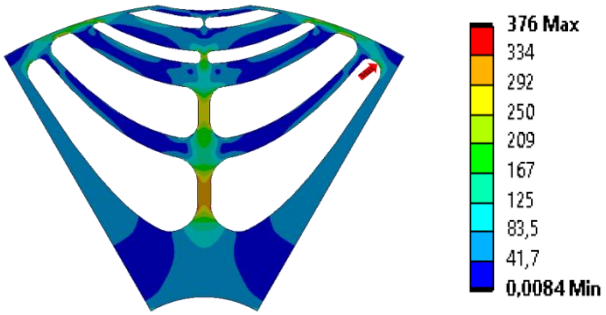

Fig. 4. Rotor with radial ribs: Equivalent von-Mises stress [MPa].

IV. Rotor Mechanical Design aided by a Topology Optimization Algorithm

Referring to the rotor with radial ribs (Fig. 4), the ribs are affected by the higher stress values, therefor the ribs thickness has been increased. It is worth recalling that the lower is the thickness of the ribs, the higher is their saturation, and then the higher are the motor performance. The idea is to reduce the ribs thickness in tangential and radial ribs by increasing their number in order to achieve an improved distribution of the mechanical load.

To improve the performance of the machine, a complete magneto-structural optimization of the rotor is desirable. In order to achieve that, a complex and heavily parameterized model would be needed to represent all the possible geometries; this strongly penalizes the speed of the optimization process. It seems relevant to obtain any possible hints on the optimal geometry to setup the most appropriate model for the magneto-structural optimization.

The optimization of the thickness and the positioning of the ribs seems to match the capabilities of the class of algorithms referred in mechanics as "Topology Optimizers" [33], [34].

These algorithms are usually adopted to optimize the quantity and the positioning of the mass needed by a mechanical part to sustain the load. Moreover, in literature there are few examples of the TO used for the design of the SynRel. Sato in [35] uses the TO optimization with a normalized Gaussian network, but in this work only the average torque and the steel losses are considered. Watanabe in [36] focuses on the torque ripple with an ON/OFF TO, but he designs the machine considering only the electromagnetic performance. There are more works for other types of machines. Lee in [37] uses the TO for the refinement of the electromagnetic performance of a Switched reluctance motor, but he considers a linear material. Instead, Garibaldi in [38] applies the principles of the TO in the multiphysics design of a Surface Mounted PM motor considering the energetic aspects, without considering the torque ripple of the machine. Further studies are necessary to use a magneto-structural TO on the SynRel machine in order to consider both the non-linearity of the material, the evaluation of the torque ripple and the maximum stress in the steel.

Here, a FE topology optimization has been used to investigate the optimal positioning and thickness of the ribs attempting to minimize the mass inside the rotor barriers. The constraints imposed are the same maximum stress and the same deformation at the airgap of the analysis in Section III.

The TO method adopted in this study is the Solid Isotropic Microstructural (or Material) with Penalization for intermediate densities (SIMP) method available in a commercial tool. It is sometimes called "material interpolation", "artificial material", "power law" or "density" method.

This method decomposes the solid part in a finite number of elements, referred to as microstructures and usually defined through the application of a mesh. The properties of each element are manipulated basing on a properly defined density ρ [34].

When the element has the properties of the solid material, the density is defined as $\rho=1$; contrarily, when the element has the properties of the air it is identified by $\rho=0$. When the element has a density in the range $0<\rho<1$, its mechanical properties are between the ones of steel and air.

Initially, the method assigns the same density to all the elements and performs a mechanical analysis in order to evaluate the sensitivity of the density of each element respect to the objective function. Basing on the sensitivity analysis, the algorithm modifies the density of each element and repeats that until the algorithm reaches the convergence.

At the end of the iterative process, the algorithm should return elements with densities $\rho=0$ (empty element) or $\rho=1$ (solid element). Even if the optimal mechanical solution could consist of mostly elements with a density $0<\rho<1$, the so called "grey" elements, they are not feasible in practice.

In order to obtain only empty and solid elements, the grey elements are penalized through a penalty coefficient γ affecting the mechanical properties of the elements. The application of the penalty coefficient related to the Young modulus is reported in (3) as an example.

$$E(\rho) = E_0 \rho^{\gamma} \tag{3}$$

where:
$E(\rho)$ is the Young modulus of the element;
E_0 is the Young modulus of the adopted steel.

Setting the penalty coefficient to infinite, the solution will not have grey elements, but the convergence of the solution might not be reached. Typical values for the penalty coefficient are in the range from 3 to 9.

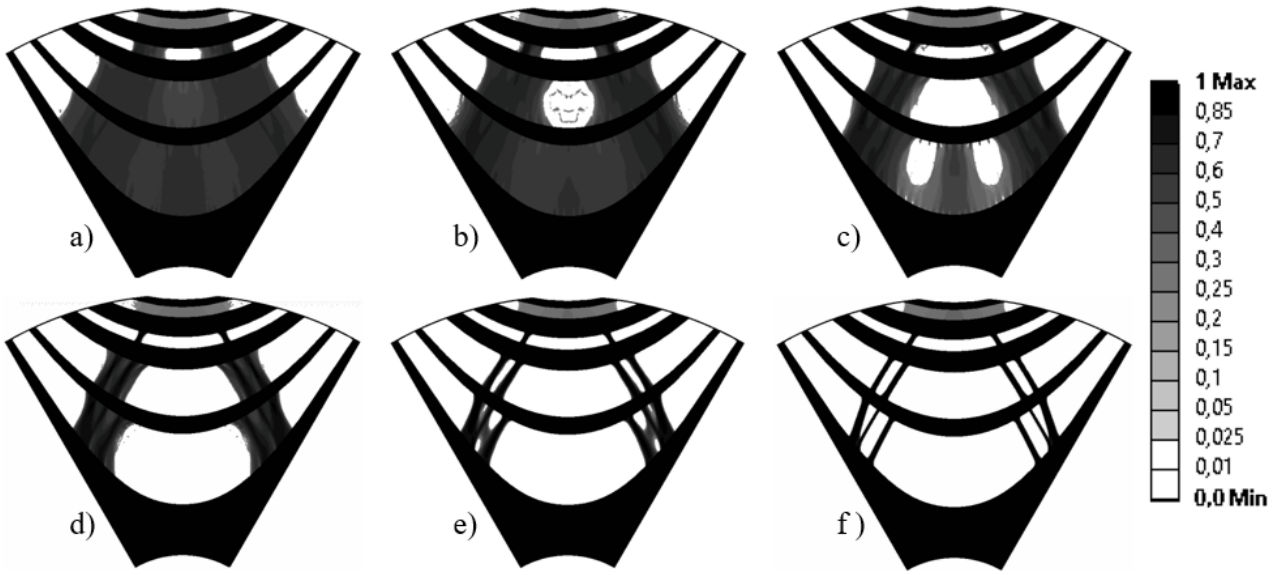

Fig. 5. Evolution of the geometry obtained with the topology optimization. Empty elements (White), "grey" elements (Grey), solid elements (Black).

Fig. 5 reports different steps of the optimization algorithm, showing how the TO modifies the density of the elements in order to distribute the stress by adopting only empty and solid elements. Fig. 5 a)-f) represent the progressing steps up to the final results.

The resulting geometry has achieved the goal to reduce the thickness of the ribs, finding a conceivable but unusual geometry, where further refinements are needed because:

1) the TO has only considered the mass distribution to counteract the centrifugal forces and not the electromagnetic performance of the machines;
2) the geometry of the fourth barrier has not been solved by the TO;
3) the resulting rotor shape has 6 interior ribs in the first barrier, but two of them are too thin to be manufactured; for this reason, the number of the internal ribs needs to be reduced to 4.

The investigation carried out by the TO provides useful guidelines about the preliminary design of the inner ribs in terms of quantity, positioning, inclination and thickness.

Therefore, the TO results can be adopted to build up a suitable parametric model to be used in a magneto-structural optimization performing independent structural and electromagnetic analyses at each optimization step.

By reducing the problem to half rotor pole for symmetry, each inner rib is described by three variables: position inside the barrier, inclination and thickness. Only the thickness defines the rib in the fourth barrier. The model reaches a total of 20 variables by including the thickness of the tangential ribs. The objective function and the constraints are listed in Table IV. The maximum allowed stress inside the rotor has been fixed at 360 MPa using a safety coefficient of 1.5; this value is considered acceptable for the operating condition of the motor.

TABLE IV
CONSTRAINTS AND OBJECTIVE FUNCTION

Constraints and objective function		**Value**
Peak Torque @ 5000 rpm	Nm	>380
Phase voltage @ 5000 rpm	V	<400
Torque ripple @ 5000 rpm	%	<10
Phase voltage @ 18000 rpm	V	<400
Motor mass (active materials)	kg	<48
Maximum equivalent von Mises stress @ 18000 rpm	MPa	<360
Objective: Maximization of the Torque @ 18000 rpm		

The whole design process has led to a new rotor layout with multiple ribs in different positions with respect to the flux barriers (Fig. 6): a quite original geometry compared to the literature ones.

The magneto-structural optimization furtherly improved the TO results in terms of thickness, positioning and inclination of the inner ribs. The mechanical equivalent von Mises stress map at the maximum speed (18000 rpm) is reported in Fig. 7 and the maximum stress values are close to those in Fig. 4; from a mechanical point of view, the two designs have similar performance.

The design steps carried out to achieve the final design of high-speed SynRels aided by a TO are summarized in Fig. 8.

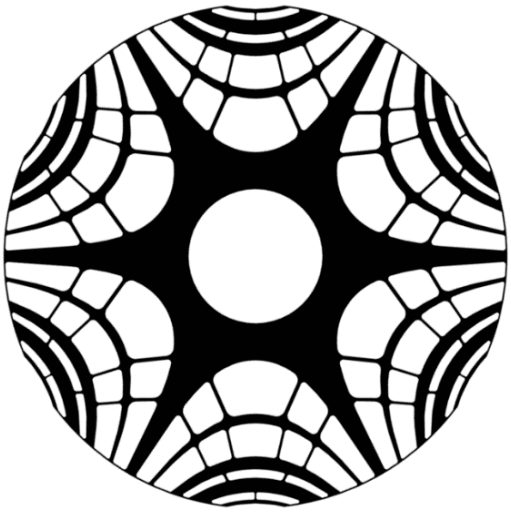

Fig. 6. Cross section of the new rotor shape.

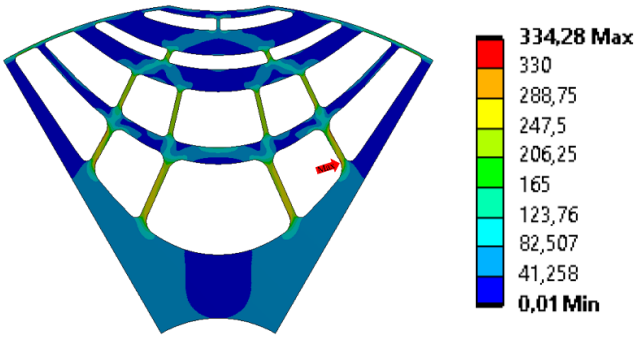

Fig. 7. Optimized rotor: Equivalent von Mises stress [MPa].

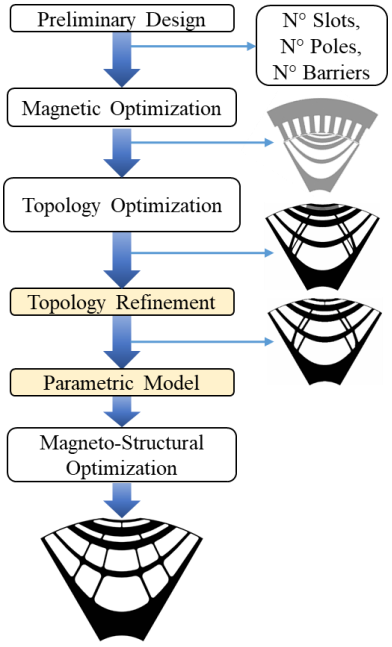

Fig. 8. Design flow involving the adoption of the Topology Optimization.

V. Results and Discussion

In this section the three rotor layouts are analyzed and compared: namely, the optimal electromagnetic design with no radial ribs (Fig. 3), the design with radial ribs (Fig. 4) and the design with optimized ribs (Fig. 6).

Fig. 9 shows the deformation of the rotor at the airgap at the maximum operating speed. The deformation is within 10% of the airgap, ensuring enough margin to avoid the contact between the rotor and the stator. Even if the optimized design has a slightly greater deformation than the radial ribs solution, this is of minor relevance because of its reduced value when compared to the airgap length. Each design assures the needed clearance between the stator and the rotor; moreover, the maximum deformation is reached in the center of the pole (in correspondence of the notch), where the airgap results increased. The deformations in the notch are not critical while outside the notch the optimized solution has a lower deformation than the radial ribs one. Otherwise, the magneto-structural optimization should include the maximum deformation at the airgap as a further constraint to assure the needed clearance.

Fig. 10 presents the saliency ratio over the speed range at the maximum performance of the machine varying the ribs layout. These results confirm a better distribution of the flux all over the speed range when the optimized ribs are used compared to the solution with radial ribs, while the "ideal" design with no ribs is still far to be equaled.

Fig. 11 and Fig. 12 report the behaviors of the d-axis and q-axis inductances related to the different layouts of the rotor. Both the inductances (L_d and L_q) tend to increase when the ribs are included inside the barriers, and thus increasing the voltage drops into the motor. The adoption of the optimized ribs strongly reduces the values of the inductances in the flux weakening operations with respect to the classical radial rib solution. The flux weakening strategy becomes easier due to the reduced voltage demanded by the motor at high speeds and the motor performance increases.

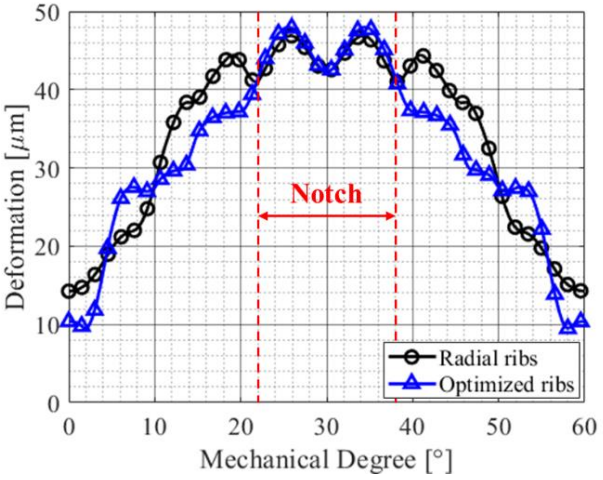

Fig. 9. Deformation at the airgap of the SynRel rotor: radial ribs vs optimized ribs at maximum speed.

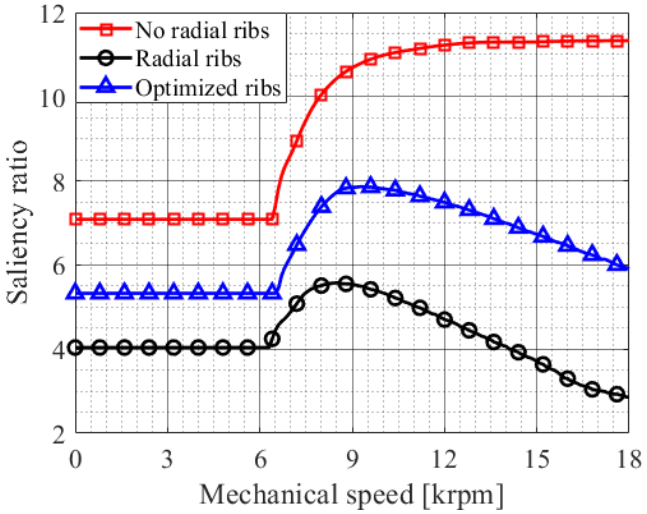

Fig. 10. Saliency ratio over the speed range for the rotor with no radial ribs, with radial ribs and with optimized ribs.

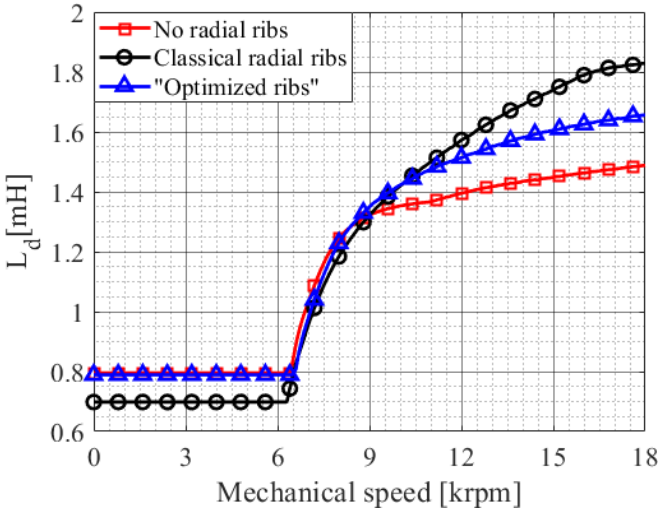

Fig. 11. D-axis inductances over the speed range for the motor with no radial ribs, with radial ribs and with optimized ribs.

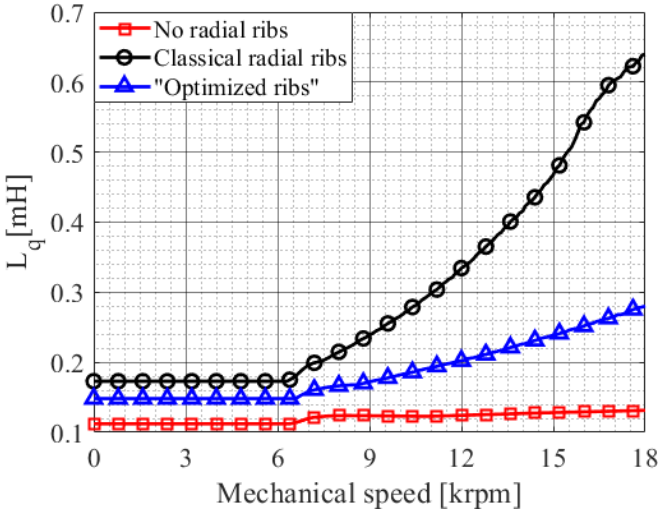

Fig. 12. Q-axis inductance over the speed range for the motor with no radial ribs, with radial ribs and with optimized ribs.

Fig. 13 and Fig. 14 show the performance of the motor over the speed range respectively in terms of torque and power varying the adopted ribs layout. The new rotor solution allows to gain up to 65% more power at high speed with respect to the layout with radial ribs. Other performances are listed in Table V, in particular the optimized layout gives also benefits for the power factor, for the efficiency and for the torque ripple.

Despite the complexity of the optimized geometry, no additional cost associated or manufacturing concerns are expected compared to the other presented geometries.

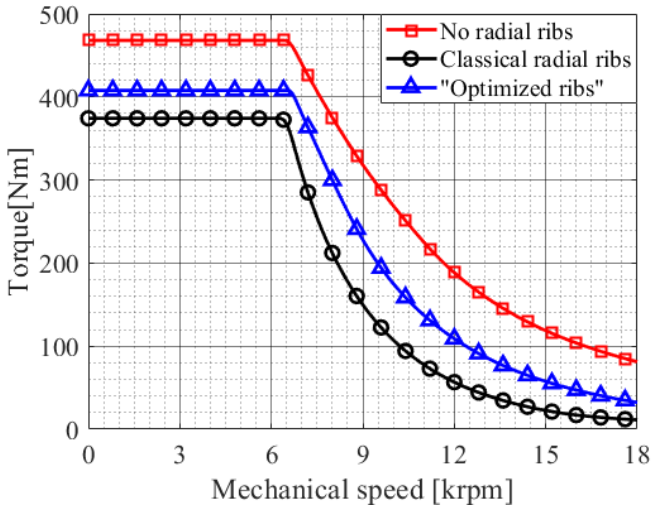

Fig. 13. Electromagnetic torque over the speed range for the motor with no radial ribs, with radial ribs and with optimized ribs.

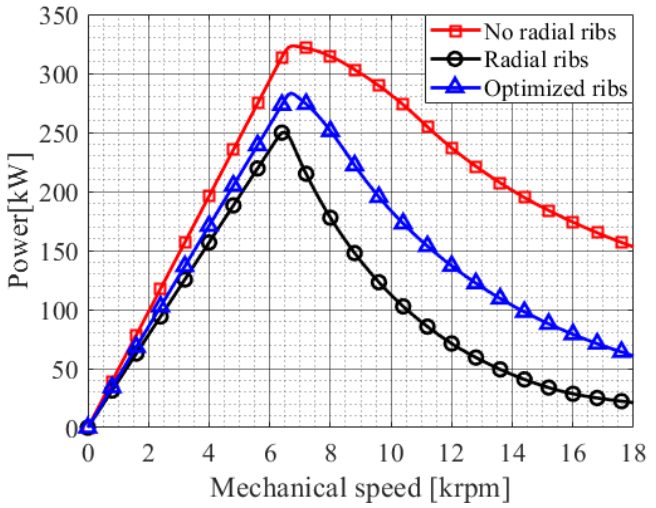

Fig. 14. Output Power over the speed range for the motor with no radial ribs, with radial ribs and with optimized ribs.

TABLE V
COMPARISON OF THE PROPOSED SOLUTIONS

Performance		**no radial ribs**	**radial ribs**	**optimized ribs**
Peak torque	Nm	430	358	384
Peak power	kW	287	230	250
Peak efficiency	%	97.6	96.9	97.1
Power @ max speed (18000 rpm)	kW	110	35	58.5
Power factor @ 200kW		0.64	0.46	0.51
Power factor @ max speed		0.61	0.41	0.46
Torque ripple @ max power	%	8	14	10
Max deformation @ airgap	%	-	6.6	7.4
Max equivalent von Mises stress	MPa	-	364	361

VI. CONCLUSIONS

Different types of motors are under evaluation for traction applications in e-mobility. Synchronous Reluctance Motors are becoming of great interest in the recent years and represent a suitable alternative for their simple and rugged construction. In this study, different solutions have been proposed and compared, with particular focus on the coupled electromagnetic and mechanical design aspects. Since the SynRel is designed with a small airgap and its rotor geometry is mechanically weak, the containment of themechanical stress and of the deformation of the rotor is challenging at high speeds. Hence, in this study a deep geometry optimization has been carried out with the aim to refine the rotor shape in order to achieve a better trade-off between the rotor integrity and the motor performance. To this extent, a Topology Optimization has been used in order to obtain the guideline for the optimal positioning and thickness of the ribs, detailing the impact on the performance. The SynRel motor may not guarantee the same peak performances of IM and PM motors in automotive applications, especially when a high speed is required. Nevertheless, an accurate design can fill the gaps of other technologies and, when the cost aspect is relevant, it can be a valid solution. In particular, the Synchronous Reluctance motor represents a potential candidate to reduce the use of rare-earth materials in large mass production scenarios.

ACKNOWLEDGMENT

This project (ReFreeDrive) has received funding from the European Union's Horizon 2020 research and innovation programme under the Grant Agreement No (770143).

REFERENCES

[1] A. Credo, G. Fabri, M. Villani and M. Popescu, "High Speed Synchronous Reluctance Motors for Electric Vehicles: a Focus on Rotor Mechanical Design", *IEEE International Electric Machines & Drives Conference (IEMDC)*, 2019.

[2] C.C.Chan, "The State of the Art of Electric and Hybrid Vehicles", *Proceeding of IEEE*, vol. 90, no. 2, February 2002, pp. 247-275.

[3] Z. Q. Zhu, D. Howe, "Electrical Machines and Drives for Electric, Hybrid, and Fuel Cell Vehicles", *Proceedings of the IEEE*, vol. 95, no. 4, April 2007, pp. 746-765.

[4] J.R. Hendershot and T.J. E. Miller, Design of Brushless Permanent-Magnet machines, *Motor Design Books LLC*, 2010.

[5] K. T. Chau, C. C. Chan, Chunhua Liu, “Overview of Permanent-Magnet Brushless Drives for Electric and Hybrid Electric Vehicles”, *IEEE Transaction on Industrial Electronics*, vol. 55, no.. 6, June 2008, pp. 2246-2257.

[6] E. Arfa Grunditz, T. Thiringer, “Performance Analysis of Current BEVs Based on a Comprehensive Review of Specifications“, *IEEE Trans. On Transportation Electrification*, Vol. 2, No. 3, September 2016.

[7] I. Boldea, L. Tutelea, L. Parsa and D. Dorrell, "Automotive Electric Propulsion Systems With Reduced or No Permanent Magnets: An Overview", *IEEE Transactions on Industrial Electronics*, vol. 61, no. 10, pp. 5696-5711, 2014.

[8] J. D.Widmer , R. Martin, M. Kimiabeigi, “Electric vehicle traction motors without rare earth magnets”, *Sustainable Materials and Technologies, Elsevier*, 3 (2015), pp. 7-13.

[9] Online database www.evspecifications.com

[10] G. Pellegrino, T. Jahns, N. Bianchi, W. Soong and F. Cupertino, The Rediscovery of Synchronous Reluctance and Ferrite Permanent Magnet Motors, *Springer International Publishing*, 2016.

[11] M. Villani, M. Tursini, M. Popescu, G. Fabri, A. Credo, L. Di Leonardo “Experimental Comparison between Induction and Synchronous Reluctance Motor-Drives” *ICEM 2018, XXIII International Conference on Electrical Machines, Alexandroupoli (Greece)*, September 2018.

[12] C. Oprea, A. Dziechciarz and C. Martis, "Comparative analysis of different synchronous reluctance motor topologies", *2015 IEEE 15th International Conference on Environment and Electrical Engineering (EEEIC)*, 2015.

[13] C. Babetto, G. Bacco and N. Bianchi, "Synchronous Reluctance Machine Optimization for High-Speed Applications", *IEEE Transactions on Energy Conversion*, vol. 33, no. 3, pp. 1266-1273, 2018.

[14] M. Ferrari, N. Bianchi, A. Doria and E. Fornasiero, "Design of Synchronous Reluctance Motor for Hybrid Electric Vehicles", *IEEE Transactions on Industry Applications*, vol. 51, no. 4, pp. 3030-3040, 2015.

[15] M. Tursini, M. Villani, G. Fabri, A. Credo, F. Parasiliti and A. Abdelli, "Synchronous Reluctance Motor: Design, Optimization and Validation", *SPEEDAM, International Symposium on Power Electronics, Electrical Drives, Automation and Motion, Amalfi (Italy)*, June 2018.

[16] M. Nardo, G. Calzo, M. Galea and C. Gerada, "Design Optimization of a High-Speed Synchronous Reluctance Machine", *IEEE Transactions on Industry Applications*, vol. 54, no. 1, pp. 233-243, 2018.

[17] F.Parasiliti, M.Villani “Magnetic analysis of flux barriers Synchronous Reluctance Motors” *ICEM 2008, XVIII International Conference on Electrical Machines, Vilamoura (Portugal)*, September 2008.

[18] F. Parasiliti, M. Villani, S. Lucidi and F. Rinaldi, "Finite-Element-Based Multiobjective Design Optimization Procedure of Interior Permanent Magnet Synchronous Motors for Wide Constant-Power Region Operation", *IEEE Transactions on Industrial Electronics*, vol. 59, no. 6, pp. 2503-2514, 2012.

[19] G. Pellegrino, F. Cupertino and C. Gerada, "Automatic Design of Synchronous Reluctance Motors Focusing on Barrier Shape Optimization", *IEEE Transactions on Industry Applications*, vol. 51, no. 2, pp. 1465-1474, 2015.

[20] C. Jung, "Power Up with 800-V Systems: The benefits of upgrading voltage power for battery-electric passenger vehicles", IEEE Electrification Magazine, vol. 5, no. 1, pp. 53-58, Mar. 2017.

[21] I. Boldea, L. Tutelea, “Reluctance Electric Machines: Desing and Control”, *CRC Press, Taylor & Francis Group*, 2019.

[22] S. Taghavi and P. Pillay, "A comparative study of synchronous reluctance machine performance with different pole numbers for automotive applications," *IECON 2014 - 40th Annual Conference of the IEEE Industrial Electronics Society, Dallas, TX*, 2014, pp. 3812-3818.

[23] M. Pohl and D. Gerling, "Analytical Model of Synchronous Reluctance Machines with Zhukovski Barriers", *XIII International Conference on Electrical Machines (ICEM)*, 2018.

[24] D. Gerada, A. Mebarki, N. Brown, C. Gerada, A. Cavagnino and A. Boglietti, "High-Speed Electrical Machines: Technologies, Trends, and Developments", *IEEE Transactions on Industrial Electronics*, vol. 61, no. 6, pp. 2946-2959, 2014.

[25] K. Grace, S. Galioto, K. Bodla and A. El-Refaie, "Design and Testing of a Carbon-Fiber-Wrapped Synchronous Reluctance Traction Motor", *IEEE Trans. on Ind. Applications*, vol. 54, no. 5, pp. 4207-4217, 2018.

[26] J. Ikaheimo, J. Kolehmainen, T. Kansakangas, V. Kivela and R. Moghaddam, "Synchronous High-Speed Reluctance Machine With Novel Rotor Construction", *IEEE Transactions on Industrial Electronics*, vol. 61, no. 6, pp. 2969-2975, 2014.

[27] J. Kolehmainen, "Optimal Dovetail Permanent Magnet Rotor Solutions for Various Pole Numbers", *IEEE Transactions on Industrial Electronics*, vol. 57, no. 1, pp. 70-77, 2010.

[28] A. Credo, M. Villani, M. Popescu and N. Riviere, "Synchronous reluctance motors with asymmetric rotor shapes and epoxy resin for electric vehicles," 2019 IEEE Energy Conversion Congress and Exposition (ECCE), Baltimore, MD, USA, 2019, pp. 4463-4469

[29] P. B. Reddy et al., "Performance Testing and Analysis of Synchronous Reluctance Motor Utilizing Dual-Phase Magnetic Material," *IEEE Transactions on Industry Applications*, vol. 54, no. 3, pp. 2193-2201, May-June 2018.

[30] K. Chen, W. Yu and C. Wen, "Rotor Optimization for Synchronous Reluctance Motors", *China Electrotechnical Society Transactions on Electrical Machines and Systems*, vol. 3, no. 3, pp. 279-284, 2019.

[31] E. Lovelace, T. Jahns, T. Keim and J. Lang, "Mechanical Design Considerations for Conventionally Laminated, High-Speed, Interior PM Synchronous Machine Rotors", *IEEE Transactions on Industry Applications*, vol. 40, no. 3, pp. 806-812, 2004.

[32] M. Tursini, M. Villani, G. Fabri, S. Paolini, A. Credo and A. Fioravanti, "Sensorless control of a synchronous reluctance motor by finite elements model results", *SLED IEEE International Symposium on Sensorless Control for Electrical Drive, Catania (Italy)*, September 2017.

[33] H. Eschenauer and N. Olhoff, "Topology optimization of continuum structures: A review", *Applied Mechanics Reviews*, vol. 54, no. 4, pp. 331-390, 2001. Available: 10.1115/1.1388075.

[34] G. Rozvany, "A critical review of established methods of structural topology optimization", *Structural and Multidisciplinary Optimization*, vol. 37, no. 3, pp. 217-237, 2008.

[35] S. Sato, T. Sato and H. Igarashi, "Topology Optimization of Synchronous Reluctance Motor Using Normalized Gaussian Network", *IEEE Transactions on Magnetics*, vol. 51, no. 3, pp. 1-4, 2015.

[36] K. Watanabe, T. Suga and S. Kitabatake, "Topology Optimization Based on the ON/OFF Method for Synchronous Motor", IEEE Transactions on Magnetics, vol. 54, no. 3, pp. 1-4, 2018.

[37] J. Lee, J. Seo and N. Kikuchi, "Topology optimization of switched reluctance motors for the desired torque profile", *Structural and Multidisciplinary Optimization*, vol. 42, no. 5, pp. 783-796, 2010.

[38] M. Garibaldi, C. Gerada, I. Ashcroft and R. Hague, "Free-Form Design of Electrical Machine Rotor Cores for Production Using Additive Manufacturing", *Journal of Mechanical Design*, vol. 141, no. 7, 2019.

[39] J. Jung et al., "Mechanical Stress Reduction of Rotor Core of Interior Permanent Magnet Synchronous Motor", *IEEE Transactions on Magnetics*, vol. 48, no. 2, pp. 911-914, 2012.

[40] F. Chai, Y. Li, P. Liang and Y. Pei, "Calculation of the Maximum Mechanical Stress on the Rotor of Interior Permanent-Magnet Synchronous Motors", *IEEE Transactions on Industrial Electronics*, vol. 63, no. 6, pp. 3420-3432, 2016.